Check for updates

Cite this: *RSC Adv.*, 2017, **7**, 55163

Naphthoquinone based chemosensors for transition metal ions: experiment and theory†

Prajkta Gosavi-Mirkute, ‡[a] Amit Patil, ‡[a] Dipali N. Lande, [a] Debamitra Chakravarty, [b] Shridhar P. Gejji, [a] Surekha Satpute [c] and Sunita Salunke-Gawali *[a]

The synthesis and characterization of 2-((pyridine-2-yl)methylamino)naphthalene-1,4-dione (**H-1**), 2-((thiophen-2-yl)methylamino)naphthalene-1,4-dione (**H-2**) and 2-((pyridine/thiophen-2-yl)ethylamino) naphthalene-1,4-dione (**H-3** and **H-4**) have been carried out. Molecular recognition abilities of these ligands toward transition metal ions in methanol, methanol–water, methanol–triethylamine or methanol–water–triethylamine mixtures, stoichiometries and association constants of **H-1** and **H-3** have been determined. It has been shown that **H-1** and **H-3** coordinate to metal ions *via* two nitrogen atoms and oxygen and exhibit remarkable selectivity towards Cu^{2+} ions in methanol or methanol–water mixtures, the complexation being accompanied by a color change from orange to intense blue. LOD (Limit of Detection) of Cu^{2+} with **H-1**, **H-3** are 1.48×10^{-8} mol L^{-1} and 1.59×10^{-8} mol L^{-1} respectively. The vibrational spectra, ^1H NMR chemical shifts and optical properties of **H-1** to **H-4** derived from density functional theory are also presented.

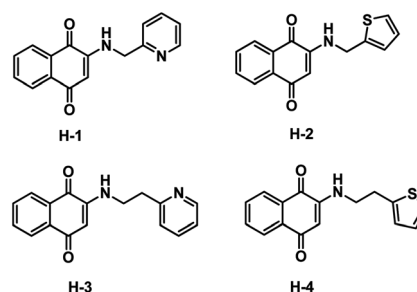## Introduction

The α,β-unsaturated carbonyl derivatives of 1,4-naphthoquinones[1] are of growing interest owing to their anticancer,[2–7] antimicrobial,[8–10] antifungal,[11–13] antitumor[14–18] and antiviral[19–21] activities. Their molecular attributes, namely conjugation and electrophilicity, govern metabolic pathways and the key processes in chemotherapy that require redox cycling drugs.[22] The underlying redox switching of such naphthoquinones, which on the acceptance of one or two electrons yield a radical anion or dianion, are thus interesting. It is further discernible to note that the intra-molecular charge transfer (ICT) transition is shown to be strongly dependent on the amine substituent and in particular, the charge density on the nitrogen center.[23] These ligands, which serve as chemosensors, have shown remarkable molecular recognition and gave easily detectable, sensitive signals. A colorimetric and ratiometric fluorescent chemosensor combined with attributes such as high fluorescence sensitivity and aesthetic appeal of colorimetric assay makes these napthoquinone sensors very fascinating.[24]

Naphthoquinone based chemosensors *viz.*, 2-((pyridin-2-yl)methylamino)naphthalene-1,4-dione (**H-1**), 2-((thiophen-2-yl)methylamino)naphthalene-1,4-dione (**H-2**) 2-((pyridine/thiophen-2-yl)ethylamino)naphthalene-1,4-dione (**H-3** and **H-4**) (Fig. 1) are synthesized and characterized using FT-IR, ^1H and ^{13}C NMR and single-crystal X-ray diffraction studies. The chemosensing ability of ligands with metal ions; La^{3+}, Hg^{2+}, Cd^{2+}, Zn^{2+}, Cu^{2+}, Cu^{+}, Ni^{2+}, Co^{2+}, Mn^{2+}, Cr^{3+} and Ca^{2+} in methanol, methanol–water mixture and in the presence of a mild base such as triethylamine has been evaluated. Moreover, the chemosensors **H-1** and **H-3** are shown to be useful for detection of different metal ions *viz.*, Cu^{2+}, Ni^{2+} and Co^{2+} revealing a color change that can be observed with the naked eye and further can be studied through the UV-visible and fluorescence experiments.

[a] *Department of Chemistry, Savitribai Phule Pune University, Pune 411007, India. E-mail: sunitas@chem.unipune.ac.in*

[b] *Central Instrumentation Facility, Department of Chemistry, Savitribai Phule Pune University, Pune 411007, India*

[c] *Department of Microbiology, Savitribai Phule Pune University, Pune 411007, India*

† Electronic supplementary information (ESI) available: FT-IR, ^1H and ^{13}C NMR, DSC are presented in Fig. S1 through Fig. S6. crystallography figures Fig. S7 and S8. Metal ion binding studies on **H-3**. Job plot for **H-1** Fig. S10 through Fig. S12. Binding constant for **H-1** Fig. S13. Job plot for **H-3** Fig. S14 through Fig. S16. Binding constant for **H-1** Fig. S17. Competative metal ion binding studies for **H-3**, Fig. S18 through Fig. S19. pH dependent binding (Fig. S20). Limit of detetion (LOD) in Fig. S21 and S22. Crystallographic Tables S1–S12. CCDC 1506931, 1575689 and 1506932 for **H-1**, **H-3** and **H-4** respectively. For ESI and crystallographic data in CIF or other electronic format see DOI: 10.1039/c7ra10490a

‡ Contributed equally.

Fig. 1 Molecular structure of **H-1**, **H-2**, **H-3** and **H-4**.

On the other hand, **H-2** and **H-4** do not show any chemosensing ability toward the metal ions studied herein.

Experimental

Materials and methods

1,4-napthoquinone, 2-methoxy-1,4-napthoquinone, 2-picolyl amine, 2-thiophenemethylamine, 2-(2′-aminoethyl)pyridine, 2-thiopheneethylamine from Sigma-Aldrich; $CuCl_2 \cdot 2H_2O$, CuCl, $NiCl_2 \cdot 6H_2O$, $ZnCl_2$, $HgCl_2$, $CoCl_2$, $CaCl_2$, triethylamine, methanol and dichloromethane from Merck chemicals; $FeCl_3 \cdot 6H_2O$ from Qualigens Chemicals, $CrCl_3 \cdot 6H_2O$, $CdSO_4$, $MnCl_2 \cdot 4H_2O$ from Fluka; $LaCl_3 \cdot 7H_2O$ from Thomas and Baker were obtained. Milli-Q water was used for preparation of aqueous solutions. Anhydrous methanol was prepared by literature reported procedure.[25] FT-IR spectra (Fig. S1 in ESI†) were recorded between 4000 and
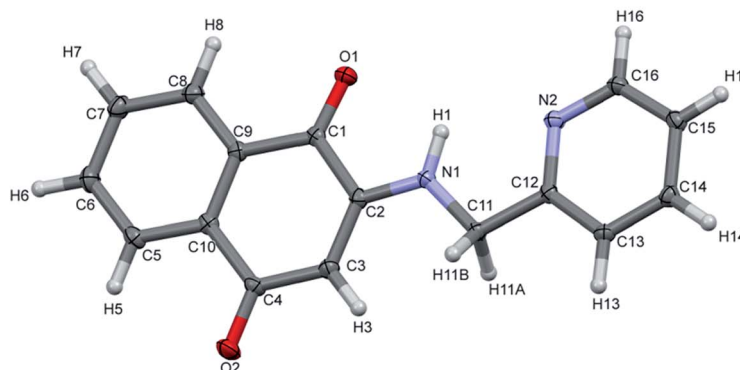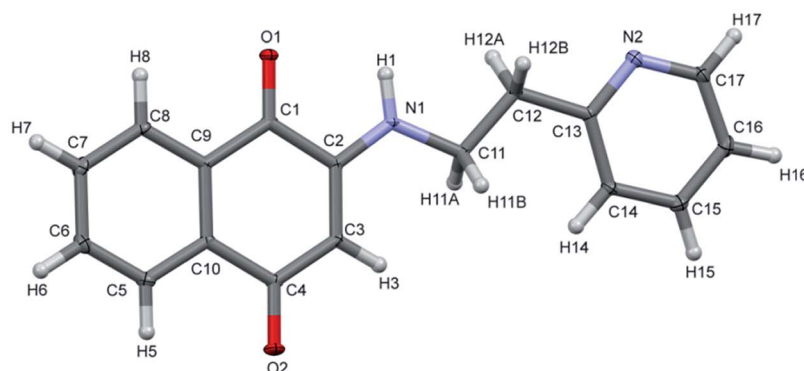
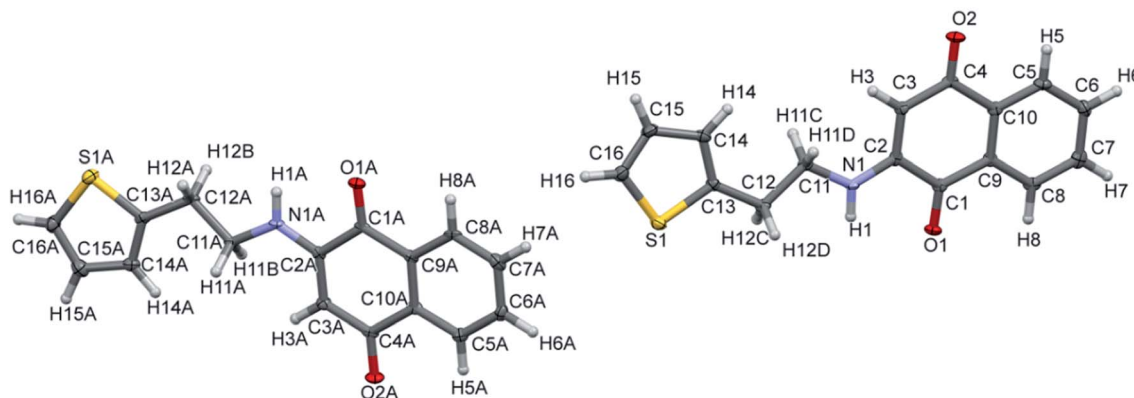**Fig. 2** ORTEP of **H-1**, **H-2**, **H-3** and **H-4**. The ellipsoid was drawn with 50% probabilities.

400 cm^{-1} as KBr pellets on SHIMADZU FT 8400 and Bruker FT-IR Spectrophotometers. The elemental analysis was performed on Thermo Finnigan EA 1112 Flash series Elemental Analyzer. ^{1}H and ^{13}C NMR (Fig. S2–S5 in ESI†) were obtained in DMSO-d_6, with the help of Varian Mercury NMR spectrometer using the TMS (tetramethylsilane) as a reference. UV-vis spectra were measured on the SHIMADZU UV 1650 in DMSO between 200 nm to 800 nm. The fluorescence spectra were recorded on JASCO spectrofluorometer FP-8300. Melting points were observed using the DSC experiments on TA waters model Q2000 instrument (Fig. S6 in ESI†) equipped with Tzero aluminium pan as a sample holder.

Synthesis of 2-((pyridin-2-yl)methylamino)naphthalene-1,4-dione (H-1). 1 mmol of 2-methoxy-1,4-naphthoquinone (0.2 g) was dissolved in 20 ml dry methanol and dichloromethane (5 ml). The solution was stirred for 20 minutes at room temperature (26 °C). To this solution 0.11 ml of 2-picolyl amine (1 mmol) was added drop wise with constant magnetic stirring. The reaction mixture was stirred for 24 hours at room temperature (26 °C) and further refluxed for 2 days at 60 °C. Completion of the reaction was monitored on TLC (toluene : methanol) with a color change from yellow to orange. The mixture after refluxing was further kept for 24 hours for evaporation of solvent which yield the red colored crystals.

Synthesis of 2-((thiophen-2-yl)methylamino)naphthalene-1,4-dione (H-2). 1 g of 1,4-naphthoquinone (6.32 mmol) was taken in two necked round bottom flask. About 20 ml dry methanol was added to just dissolve it. The solution was stirred for 15 min on a magnetic stirrer. To this solution 0.64 ml (6.4 mmol) of 2-thiophenemethylamine was added drop wise. The reaction mixture was stirred for 24 hours at room temperature (26 °C) with a constant magnetic stirring and the completion of the reaction was monitored on TLC. After 24 hours the mixture was transferred to a beaker and kept for 24 to 48 hours so that the solvent evaporates. A solid crude product was obtained by evaporation was purified by column chromatography with toluene : methanol (9 : 1) as eluent. A red colored product was obtained subsequent to a slow evaporation of eluent.

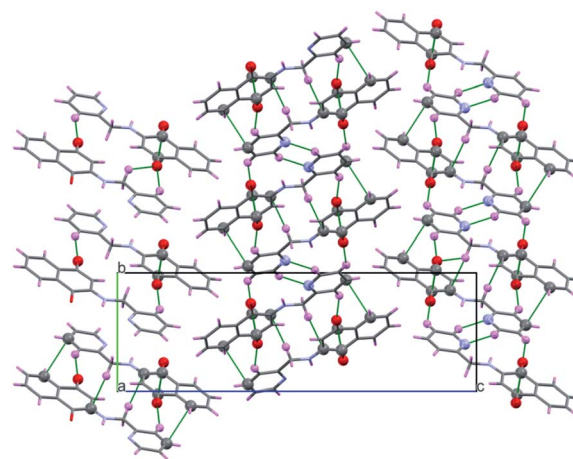**Synthesis of 2-((pyridine/thiophen-2-yl)ethylamino) naphthalene-1,4-dione (H-3 and H-4).** 1 g of 1,4-naphthoquinone

Fig. 3   Polymeric chains of **H-1** molecules down *a*-axis.

Table 1 Single crystal X-ray data for **H-1**, **H-3** and **H-4**

Identification code	**H-1**	**H-3**	**H-4**
Empirical formula	$C_{16}H_{12}N_2O_2$	$C_{17}H_{14}N_2O_2$	$C_{16}H_{13}NO_2S$
Formula weight	264.28	278.3	283.33
Temperature	100(2) K	100(2) K	100(2) K
Wavelength	0.71073 Å	0.71073 Å	0.71073 Å
Crystal system	Monoclinic	Monoclinic	Triclinic
Space group	$P2_1/n$	$P2_1/n$	$P\bar{1}$
Unit cell dimensions	$a = 5.7063(4)$ Å	$a = 5.4000(4)$ Å	$a = 5.4069(5)$ Å, $\alpha = 92.338(4)°$
	$b = 8.4245(6)$ Å, $\beta = 93.229(2)°$	$b = 30.026(2)$ Å, $\beta = 99.278(2)°$	$b = 8.0971(7)$ Å, $\beta = 91.024(4)°$
	$c = 25.6881(19)$ Å	$c = 8.0578(6)$ Å	$c = 29.735(3)$ Å, $\gamma = 98.992(4)°$
Volume	1232.94(15) Å^3	1289.39(17) Å^3	1284.3(2) Å^3
Z	4	4	4
Density (calculated)	1.424 Mg m^{-3}	1.434 Mg m^{-3}	1.465 Mg m^{-3}
Absorption coefficient	0.096 mm^{-1}	0.096 mm^{-1}	0.252 mm^{-1}
F(000)	552	584	592
Crystal size	0.34 × 0.26 × 0.24 mm^3	13.000 × 0.210 × 0.070 mm^3	0.41 × 0.21 × 0.04 mm^3
Theta range for data collection	2.893 to 28.388°	2.713 to 28.345°	2.841 to 28.611°
Index ranges	$-7<=h<=7$, $-11<=k<=11$, $-34<=l<=34$	$-7<=h<=7$, $-40<=k<=40$, $-10<=l<=10$	$-7<=h<=7$, $-10<=k<=10$, $-39<=l<=37$
Reflections collected	48 104	51 719	24 810
Independent reflections	3076 [$R(int) = 0.0306$]	3213 [$R(int) = 0.0643$]	6062 [$R(int) = 0.0555$]
Completeness to theta = 25.242°	99.90%	99.90%	97.60%
Refinement method	Full-matrix least-squares on F^2	Full-matrix least-squares on F^2	Full-matrix least-squares on F^2
Data/restraints/parameters	3076/0/181	3213/0/191	6062/0/361
Goodness-of-fit on F^2	1.032	1.054	1.155
Final R indices [$I > 2sigma(I)$]	$R_1 = 0.0393$, w$R_2 = 0.1039$	$R_1 = 0.0610$, w$R_2 = 0.1054$	$R_1 = 0.0926$, w$R_2 = 0.2044$
R Indices (all data)	$R_1 = 0.0445$, w$R_2 = 0.1079$	$R_1 = 0.0784$, w$R_2 = 0.1114$	$R_1 = 0.1233$, w$R_2 = 0.2187$
Extinction coefficient	n/a	0.0039(6)	n/a
Largest diff. peak and hole	0.344 and -0.273 e Å^{-3}	0.440 and -0.361 e Å^{-3}	0.756 and -0.593 e Å^{-3}

(6.32 mmol) was dissolved in 25 ml methanol and mixture stirred for about 20 min. To this solution 0.70 ml of 2-(2′-aminoethyl) pyridine (7.1 mmol) for **H-3** and 0.69 ml of 2-thiopheneethylamine (7.1 mmol) for **H-4** were added drop wise. The reaction mixture was stirred for 24 hours at room temperature (26 °C) with constant magnetic stirring till completion of the reaction monitored on TLC. The reaction mixture was evaporated under the reduced pressure. The residue was column chromatographed over silica gel in methanol/toluene (1 : 9) solvent system. Red coloured solid products were obtained after evaporation of pure fraction from the column.

Characterization

2-((Pyridin-2-yl)methylamino)naphthalene-1,4-dione;   H-1.
Dark red colour crystal. Yield: 0.174 g (62.14%). mp 156.42 °C. Anal. data calcd for $C_{16}H_{12}O_2N_2$ (%): C, 72.99; H, 4.21; N, 10.64. Found (%): C, 72.68; H, 4.10; N, 10.32. FT-IR (KBr; ν_{max} (cm^{-1})): 3355, 3061, 1672, 1632, 1605, 1593, 1563, 1432, 1373, 1347, 1290, 1214, 1158, 1122, 1091, 1049, 976, 827, 778, 757, 723, 669, 574, 498, 460, 443. ^{1}H NMR (DMSO-d_6, 499.81 MHz, δ (ppm)): 4.52 (d, J = 6 Hz, 2H, –CH$_2$), 5.59 (s, 1H, Ar–CH), 7.30 (t, J = 5 Hz, 1H, Ar), 7.37 (d, J = 8 Hz, 1H, Ar), 7.73 (t, J = 8 Hz, 1H, Ar), 7.77 (m, J = 8 Hz, 1H, Ar), 7.81 (m, J = 7.5 Hz, 1H, Ar), 7.90 (d, J = 8 Hz, 1H, Ar), 8.00 (d, J = 8 Hz, 1H, Ar), 8.08 (t, J = 6.5 Hz, 1H, –NH), 8.55 (d, J = 5 Hz, 1H, Ar). ^{13}C NMR (DMSO-d_6, 125.69 MHz, δ (ppm)): 47.40, 101.09, 121.98, 123.00, 125.82, 126.39, 130.86, 132.77, 133.47, 135.32, 137.47, 148.87, 149.49, 156.80, 181.95. UV-vis, (λ_{max}, methanol (nm)): 440.

2-((Thiophen-2-yl)methylamino)naphthalene-1,4-dione; H-2.
Brown colored solid. Yield: 0.962 g (89.90%). mp 189.73 °C. Anal. data calcd for $C_{15}H_{11}O_2NS$ (%): C, 66.89; H, 4.11; N, 5.20; S, 11.90. Found (%) C, 66.44; H, 3.84; N, 5.16; S, 11.65. FT-IR (KBr; ν_{max} (cm^{-1})): 3354, 1670, 1599, 1506, 1453, 1429, 1306, 1252, 1216, 1147, 1056, 1025, 835, 778, 708, 687, 627, 557, 542, 493, 444. ^{1}H NMR (DMSO-d_6, 499.81 MHz, δ (ppm)): 4.16 (s, 2H, –CH$_2$), 5.74 (s, 1H, Ar–CH), 6.97 (t, J = 4.5 Hz, 1H, Ar), 7.10 (d, J = 2.5 Hz, 1H, Ar), 7.40 (d, J = 4.5 Hz, 1H, Ar), 7.71 (t, J = 7.5 Hz, 1H, Ar), 7.80 (t, J = 7 Hz, 1H, Ar), 7.90 (d, J = 7.5 Hz, 1H, Ar), 7.97 (d, J = 7.5 Hz, 1H, Ar), 8.11 (t, J = 6.5, 1H, –NH). ^{13}C NMR (DMSO-d_6, 125.69 MHz, δ (ppm)): 40.42, 100.67, 125.31, 125.33, 125.86, 126.10, 126.75, 130.32, 132.27, 132.87, 134.82, 140.38, 148.00, 181.48, 181.53. UV-vis, (λ_{max}, methanol (nm)): 435.

2-((Pyridin-2-yl)ethylamino)naphthalene-1,4-dione;   H-3.
Dark red color crystal. Yield: 1.126 g (64.01%). mp 128.58 °C. Anal. data calcd for $C_{17}H_{14}O_2N_2$ (%): C, 73.36; H, 5.07; N, 11.49. Found (%): C, 72.98; H, 5.10; N, 11.36. FT-IR (KBr, ν_{max} (cm^{-1})): 3336, 3043, 2960, 2914, 2868, 1772, 1672, 1600, 1570, 1518, 1467, 1435, 1356, 1284, 1261, 1215, 1155, 1103, 1057, 1022, 983, 862, 785, 721, 669, 596, 559, 507, 476. ^{1}H NMR (DMSO-d_6, 499.81 MHz, δ (ppm)): 3.04 (t, J = 5 Hz, 2H, –CH$_2$), 3.54 (t, J = 5 Hz, 2H, –CH$_2$), 5.71 (s, 1H, Ar), 7.23 (t, J = 5 Hz, 1H, Ar), 7.32 (d, J = 5 Hz, 1H, Ar), 7.62 (t, J = 5 Hz, 1H, –NH), 7.705 (t, J = 5 Hz, 1H, Ar), 7.72 (t, J = 5 Hz, 1H, Ar), 7.81 (t, J = 10 Hz, 1H, Ar), 7.92 (d, J = 5 Hz, 1H, Ar), 7.95 (d, J = 10 Hz, 1H, Ar), 8.51 (d, J = 5 Hz, 1H, Ar). ^{13}C NMR (DMSO-d_6, 125.69 MHz, δ (ppm)): 35.34, 41.61, 99.51, 121.69, 123.35, 125.31, 125.85, 130.32, 132.14, 133.10,

134.82, 136.61, 148.28, 149.07, 158.66, 181.26, 181.46. UV-vis, (λ_{max}, methanol (nm)): 448.

2-((Thiophen-2-yl)ethylamine)naphthalene-1,4-dione;   H-4.
Dark red color crystals. Yield: 1.08 g (60.33%). mp 145.5 °C. Anal. data calcd for $C_{16}H_{13}O_2NS$ (%): C, 67.82; H, 4.62; N, 4.94; S, 11.31. Found (%): C, 67.58; H, 4.36; N, 5.02; S, 11.67. FT-IR (KBr, ν_{max} (cm^{-1})): 3338, 3043, 2915, 1669, 1515, 1593, 1567, 1514, 1465, 1434, 1395, 1353, 1336, 1298, 1278, 1242, 1215, 1120, 1098, 1031, 978, 859, 773, 722, 684, 583, 505, 466. ^{1}H NMR (DMSO-d_6, 499.81 MHz, δ (ppm)): 3.12 (t, J = 7 Hz, 2H, –CH$_2$), 3.45 (t, J = 6.5 Hz, 2H, –CH$_2$), 5.72 (s, 1H, Ar), 6.94 (d, J = 3.5 Hz, 1H, Ar), 6.96 (t, J = 5 Hz, 1H, Ar), 7.33 (d, J = 4.5 Hz, 1H, Ar), 7.55 (t, J = 6 Hz, 1H, –NH), 7.72 (t, J = 7.5 Hz, 1H, Ar), 7.82 (t, J = 7.5 Hz, 1H, Ar), 7.93 (d, J = 8 Hz, 1H, Ar), 7.97 (d, J = 7.5 Hz, 1H, Ar). ^{13}C NMR (DMSO-d_6, 125.69 MHz, δ (ppm)): 27.55, 43.31, 99.67, 124.27, 125.31, 125.55, 125.87, 127.00, 130.31, 132.17, 133.07, 148.24, 181.45. UV-vis, (λ_{max}, methanol (nm)): 448.

X-ray crystal structures

X-ray data for **H-1**, **H-3** and **H-4** were collected on D8 Venture PHOTON 100 CMOS diffractometer using graphite mono-chromatized Mo-Kα radiation (λ = 0.7107 Å) with exposure/frame = 10 s. The X-ray generator was operated at 50 kV and 30 mA. An initial set of cell constants and an orientation matrix were calculated from total 24 frames. The optimized strategy used for data collection included different sets of ϕ and ω scans with 0.5° steps in ϕ/ω. Crystal to detector distance was 5.00 cm with 512 × 512 pixels/frame, oscillation/frame −0.5°, maximum detector swing angle = −30.0°, beam centre = (260.2, 252.5), in plane spot width = 1.24. Data integration was carried out by Bruker SAINT program and empirical absorption correction for intensity data were carried out using the Bruker SADABS. The programs are integrated in APEX II package.[26] The data were corrected for Lorentz and polarization effect. The structure was solved by direct method using the SHELX-97 (ref. 27) with the final refinement of the structure performed by a full-matrix least-squares technique with anisotropic thermal data for non-hydrogen atoms on F^2. The non-hydrogen atoms were refined anisotropically where the hydrogen atoms were refined at the calculated positions as riding atoms with isotropic displacement parameters.[27] Molecular diagrams were generated using the ORTEP-3 (ref. 28) and Mercury programs.[29] Structural calculations were performed using SHELXTL[30] and PLATON.[31]

Metal ion binding studies, Job plot, competitive binding studies, pH studies and limit of detection (LOD) experiments

Metal ion binding studies were evaluated by following methods, (i) in methanol, (ii) in 1 : 1 methanol–water, (iii) in presence of triethylamine in (i) and (ii). In typical experiments 2 ml of **H-1** and **H-3** was mixed with 2 ml of metal ion solutions at room temperature (26 °C). 1 ml of triethylamine was added in che-mosensor solution in case of (i) and (ii) prior to addition of metal ion solutions. UV-visible and fluorescence spectra of all solutions were measured; the concentration of ~2.5 × 10^{-4} M was used.

Micromolar concentration (10–100 μM) of **H-1**, **H-3** and metal ions was used for Jobs plot experiment. Solutions were prepared

by varying concentration of ligands and metal ions. Binding constant of Cu^{2+} and Ni^{2+} was determined by Stern–Volmer plot. 5×10^{-4} M solution of chemosensor and 1×10^{-3} M metal ion solutions in methanol were used to obtained the same.

For competitive binding of metal ions (5×10^{-3} M) with **H-1** and **H-3** (5×10^{-3} M) equal volumes were mixed and fluorescence spectra of all solutions were measured.

For quantum yield experiment fluorescien is used as standard. Fluorescien (1×10^{-6} M), **H-1** and **H-3** (1×10^{-6} M) concentration is used. 0.1 M NaOH was used for the deprotonation of fluorescien.

In pH dependent metal ion binding studies experiments, 2 ml of chemosensor **H-1** and **H-3** was mixed with 2 ml of metal ion solutions (Cu^{2+}, Ni^{2+}, Zn^{2+} and Co^{2+}) at room temperature (26 °C). 2 ml of buffer solution at pH 4, pH 7 and pH 9 was added respectively prior to addition of metal ion solutions. UV-visible spectra of all solutions were measured.

Micromolar concentrations (10 to 100 μM) of **H-1**, **H-3** and Cu^{2+} metal ions were used for LOD experiments. Solutions were prepared by varying concentrations of **H-1**, **H-3** and Cu^{2+} metal ions.

Computational methodology

Optimizations of naphthoquinone derivatives were carried out using the GAUSSIAN-09 program.[32] Global hybrid meta GGA (M06-2X) functional was used in conjuction with the internally stored 6-311++G(d,p) basis set. Stationary point structures thus obtained were confirmed to be the local minima on the potential energy surfaces through vibrational frequency calculations. Frontier orbitals were derived in the same framework of theory. Electronic spectra were computed using the time dependent density functional theory (TD-DFT).

Results and discussion

Synthesis and characterization of H-1, H-2, H-3 and H-4

Chemosensor **H-1**, **H-2**, **H-3** and **H-4** were synthesized and obtained in high yields at the room temperature (26 °C) without
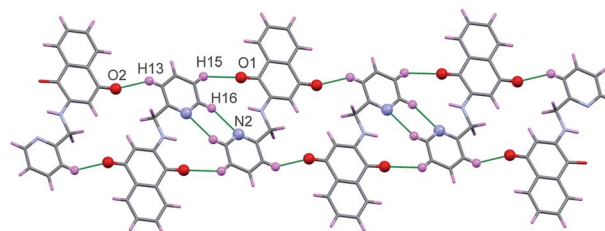

Fig. 4 Polymeric chain of **H-1** showing C–H···O and C–H···N interaction.

Table 2 Hydrogen bonding geometries of **H-1**, **H-3** and **H-4**

Compound	D–H···A	D···H (Å)	H···A (Å)	D···A (Å)	D–H···A (°)	Symmetry
H-1	N(1)–H(1)···O(1)	0.8797	2.3087(8)	2.672(1)	104.79	Intra
	C(15)–H(15)···O(1)	0.949(1)	2.5782(8)	3.363(1)	140.26(7)	2 − x, 1 − y, −z
	C(16)–H(16)···N(2)	0.950(1)	2.559(1)	3.391(1)	146.41(7)	2 − x, 1 − y, −z
	C(13)–H(13)···O(2)	0.950(1)	2.3391(8)	3.166(1)	145.14(7)	−x, −y, −z
	C(14)···C(5)			3.398(2)		(−x, −y, −z)
	C(4)···O(1)			3.216(1)		(1 − x, 1 − y, −z)
	C(1)···O(2)			3.065(1)		(−x, 1 − y, −z)
H-3	N(1)–H(1)···O(1)	0.88	2.252	3.099(1)	161.65	−x, −y, 1 − z
	N(1)–H(1)···O(1)	0.88	2.302	2.667(2)	104.91	Intra
	C(3)–H(3)···O(2)	0.951	2.511	3.446(2)	168.1(3)	2 − x, −y, 2 − z
	C(14)–H(14)···O(2)	0.949	2.633	3.564 (2)	167	2 − x, −y, 2 − z
	C(11)–H(11B)···O(2)	0.989	2.717	3.346 (2)	121.84	2 − x, −y, 2 − z
	C(12)–H(12A)···O(1)	0.99	2.658	3.211(2)	115.5	−x, −y, 1 − z
	C(12)–H(12B)···O(2)	0.99	2.624	3.421 (2)	137.64	1 − x, −y, 2 − z
	C(11)–H(11A)···C(8)	0.99	2.807	3.476(2)	125.4	1 − x, −y, 2 − z
	C(11)–H(11B)···C(3)	0.989	2.789	3.650 (2)	145.7	1 − x, −y, 2 − z
	C(4)···O(1)			3.167(2)		−1 + x, y, z
	C(1)···O(2)			3.141(7)		−1 + x, y, z
	C(1)···N(1)			3.223(2)		1 − x, −y, 1 − z
	C(13)···C(7)			3.394(2)		1 − x, −y, 1 − z
H-4	N(1)–H(1)···O(1)	0.880(4)	2.258(3)	3.104(5)	161.4(3)	2 − x, 1 − y, 2 − z
	N(1A)–H(1A)···O(1A)	0.880(4)	2.280(3)	3.121(5)	159.7(3)	1 − x, −y, 1 − z
	N(1)–H(1)···O(1)	0.88	2.307	2.670(5)	104.8	Intra
	N(1A)–H(1A)···O(1A)	0.88	2.301	2.664(5)	104.7	Intra
	C(3)–H(3)···O(2)	0.950(5)	2.649(3)	3.584(6)	168.1(3)	−x, −y, 2 − z
	C(3A)–H(3A)···O(2A)	0.951(5)	2.607(3)	3.545(6)	168.9(3)	3 − x, 1 − y, 1 − z
	C(14)–H(14)···O(2)	0.950(5)	2.504(3)	3.440(6)	168.2(3)	−x, −y, −z
	C(16)–H(16)···S(1A)	0.949(5)	2.951(3)	3.681(5)	134.7(3)	1 − x, −y, 1 − z
	C(14A)–H(14A)···O(2A)	0.950(5)	2.508(3)	3.445(6)	168.5(3)	3 − x, −y, 1 − z
	C(7)···C(13)			3.387(7)		1 − x, −y, 2 − z
	N(1)···C(1)			3.244(7)		1 − x, −y, 2 − z
	N(1A)···C(1A)			3.240(7)		2 − x, −y, 2 − z

using any exhaustive synthetic procedures. **H-1, H-2, H-3** and **H-4** were characterized by FT-IR (Fig. S1 ESI†), ^1H and ^{13}C NMR (Fig. S2 through Fig. S5 in ESI†), elemental analysis, UV-visible spectroscopy and single crystal X-ray diffraction studies. Melting point of chemosensor ligands were obtained by Differential Scanning Calorimetry (DSC) (Fig. S6 in ESI†). FT-IR spectra of the ligands reveals characteristic N–H stretching observed at the 3355 cm^{-1} (**H-1**), 3354 cm^{-1} (**H-2**), 3336 cm^{-1} (**H-3**) and 3338 cm^{-1} (**H-4**). The carbonyl frequency was assigned to the ~1672 cm^{-1} in **H-1** and **H-3**, 1670 cm^{-1} in **H-2**

and ~1669 cm^{-1} in **H-4**. The C–S frequency was observed in the range ~1467 cm^{-1} (in **H-3**) to 1432 cm^{-1} (in **H-1**).

ORTEP of **H-1, H-3** and **H-4** are shown in Fig. 2 and crystallography data have been summarized in Table 1. **H-1** and **H-3** shows the monoclinic space group while **H-4** shows triclinic space group. The carbonyl bond distances (1.21 Å and 1.23 Å) in these compounds resemble to those observed in the oxidized form of compounds. The bond distances represent quinonoid distortion with two short and four long C–C bonds. The carbonyl C(1)–O(1) and C(4)–O(2) bond distances are found to be 1.220 Å and 1.234 Å, respectively. The C(2)–N(1) bond distances (1.335 Å) match well with those of amino derivatives of 1,4-naphthoquinone.[33–38]

As may readily be noticed, **H-1** shows naphthoquinone and pyridyl rings to be coplanar (Fig. S7 in ESI†) in and render inter- as well as the intra-molecular N–H⋯O hydrogen bonding which arise from quinonoid oxygen (Table 2).

Two molecules of **H-1** oriented in the opposite directions orientations which facilitate further intermolecular C–H⋯N (C(16)–H(16)⋯N(2)) and C–H⋯O(C(15)–H(15)⋯O(1)) hydrogen bonding. Subsequently the dimeric units are linked by the C–H⋯O (C(13)–H(13)⋯O(2)) interactions along a polymeric chain down a-axis (cf. Fig. 3 and 4) facilitate C–H⋯π interactions between the alkyl proton C(11)–H(11B) and quinonoid ring; with the corresponding distance being 3.231 Å. Benzenoid carbon C(5) in close contact with neighbouring molecules pyridine ring carbon C(14) (3.398(2) Å, (1 − x, −y, −z) (cf. Fig. 5); the C(4)⋯O(1) (−1 + x, y, z) separation of neighbouring molecules was 3.216 Å.

The mutual orientation of pyridyl ring with naphthoquinone show a marginal deviation (Fig. S8 in ESI†) from the planarity as adjudged from the C(11)–N(1)–C(2)–C(1) dihedral angle parameters. A bidentate coordination of **H-3** ligand with the metal ions is favoured; as inferred earlier in ref. 39–41.

As far as **H-3** is concerned the opposite orientation was noticed (with respect pyridine ring) with a polymeric chain therein extending from one end by N(1)–H(1)⋯O(1) and C(12)–H(12A)⋯O(1), C(3)–H(3)⋯O(2), C(12)–H(12B)⋯O(2) and C(14)–H(14)⋯O(2) hydrogen bonding interactions, which are depicted in Fig. 6 and 7. Furthermore the polymeric chain brings about C–H⋯π, C⋯C(C(7)⋯C(13)), C⋯N (C(1)⋯N(1)) and C⋯O(C(4)⋯O(4)) stacking interactions as shown in Fig. 8. Besides the C–H⋯π interactions from ethyl protons and C(11)–(11A) of
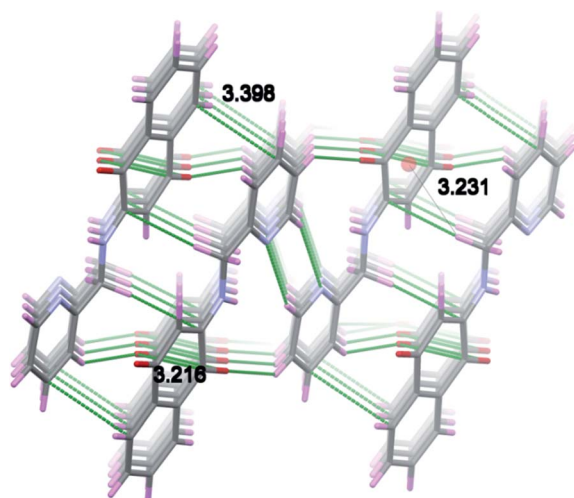

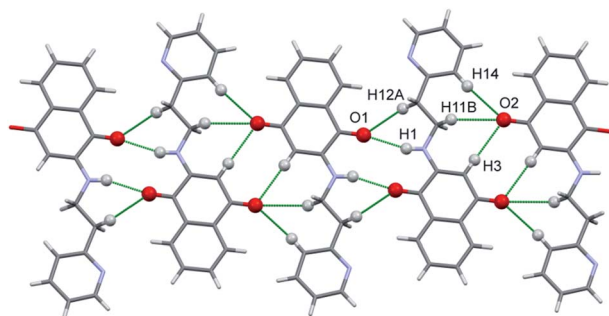**Fig. 5** Figure showing π–π stacking and C–H⋯π interactions to **H-1** molecules.

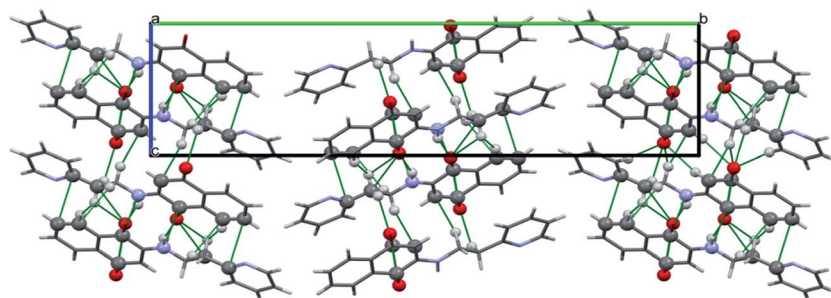**Fig. 6** Polymeric chains of **H-3** molecules down a-axis.

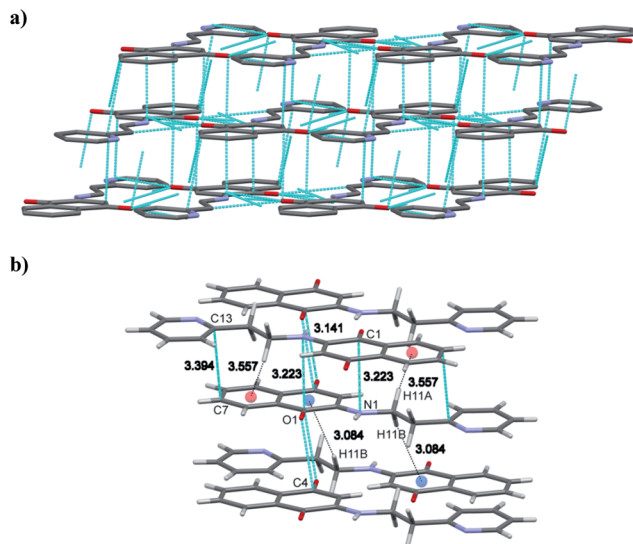**Fig. 7** Polymer chain of **H-3** showing N–H⋯O and C–H⋯O interaction.

a)

b)

Fig. 8 (a) and (b) showing π–π stacking and C–H⋯π interaction in H-3 molecule.

the benzenoid ring and those between C(12)–H(12B) and quinonoid can readily be noticed.

Unlike **H-1** and **H-3** the polymeric chains of **H-4** reveal two asymmetric molecules linked by the C(16)–H(16)⋯S(1A) $(1 − x, −y, 1 − z)$ interactions which are depicted in Fig. 9. In addition to these C(11)–H(11A)⋯π and N(1)–H(1A)⋯π interactions from the quinonoid ring are transparent. On the other hand the C(12)–H(12B)⋯π interactions bring forth the binding with benzenoid moiety as can be deciphered from Fig. 10. Subsequently the interactions between asymmetric molecules engender marginal variations in their corresponding proton distances.

Sensing metal ion binding of H-1 and H-3

No significant colour change was observed in metal ions binding studies experiments of **H-2** and **H-4**. The metal ion binding studies thus focuses on **H-1** and **H-3** ligands. Metal ion
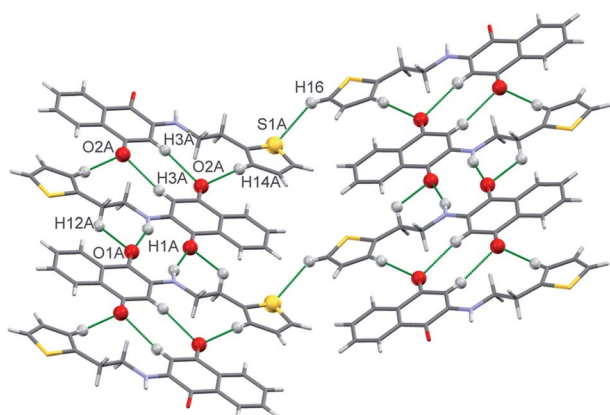

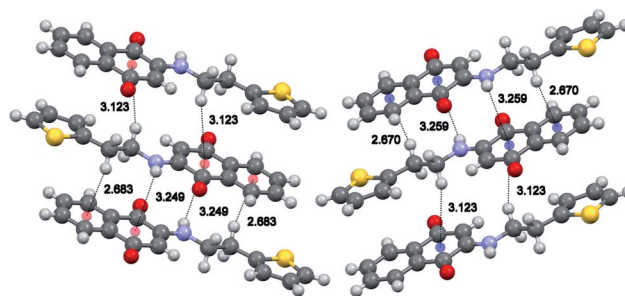**Fig. 9** Figure showing two asymmetric molecules of H-4 are joined by C–H⋯S interaction.

Fig. 10 C–H⋯π and N–H⋯π interaction of H-4 molecules.

binding studies[35] were carried out (i) in methanol (ii) in methanol–water, (iii) in presence of mild base triethylamine (TEA) in (i) and (ii) conditions. TEA was used for deprotonation of ligand for detection of metal ions.

Equal volumes of $(2.5 × 10^{−4}$ M) of different metal ion solutions were mixed with **H-1** and **H-3** in methanol at room temperature (26 °C). A color change from orange in **H-1** on addition of Cu^{2+}, Cu^+, Ni^{2+}, Zn^{2+} and Co^{2+} ions can be attributed to deprotonation of N–H of the ligand which can be visualized with the naked eye (Fig. 11). A new band appeared in the range of 500–700 nm for Zn^{2+}, Cu^{2+}, Cu^+, Ni^{2+} and Co^{2+} in the UV-visible spectra portrayed in Fig. 13a. The addition of triethylamine prior to addition of the metal ion solution, show a color change in the **H-1** (shown in Fig. 11b) only for Zn^{2+}, Cu^{2+}, Cu^+, Ni^{2+} and Co^{2+} which is accompanied by an emergence of a new band in ∼500–700 nm region (Fig. 13b).

Interestingly **H-3** only shows color change with Cu^+ and Cu^{2+} in methanol as can readily be noticed from Fig. 12a, subsequent addition of triethylamine led to binding with Cu^+, Cu^{2+}, Ni^{2+} and Co^{2+} ions concomitantly bringing about the color change for **H-3** as evident from Fig. 12b (and also Fig. S9 shown in ESI†).

Fig. 11c displays **H-1** in the 1 : 1 mixture of methanol–water. Here the color change from yellow to grey was noticed only for the Cu^{2+}. No color change was observed for the rest of the metal ions studied. In other words, **H-1** selectively detects Cu^{2+} ion in methanol–water solvent mixture with the naked eye. Similar inferences are drawn for the **H-3** ligand shown in Fig. 12c.

As inferred from Fig. 11d and 12d; **H-1** and **H-3** do not show any noticeable color change for triethylamine and methanol–water solvent mixtures. On addition of Ni^{2+} and Zn^{2+} solution the UV-visible spectra emerge with new bands near λ_{max} 340 nm and 360 nm displayed in Fig. 13d and Fig. S9d in ESI.†

Competitive binding, pH dependent binding studies and detection limit of H-1 and H-3

The stoichiometry of **H-1** (Fig. S10 through Fig. S12 in ESI†) and **H-3** (Fig. S14 through Fig. S16 in ESI†) for Cu^{2+}, Ni^{2+} was determined by the Job's plot method. As illustrated **H-1** with Cu^{2+} showed 1 : 1 stoichiometry in methanol as well as methanol–water mixtures, whereas the 2 : 1 stoichiometry was suggested for the Ni^{2+} in methanol (Fig. S10 in ESI†). Besides Cu^{2+} in methanol–water–triethylamine mixture (Fig. S11 in ESI†) revealed 2 : 1 stoichiometry. Likewise the **H-3** on combining with
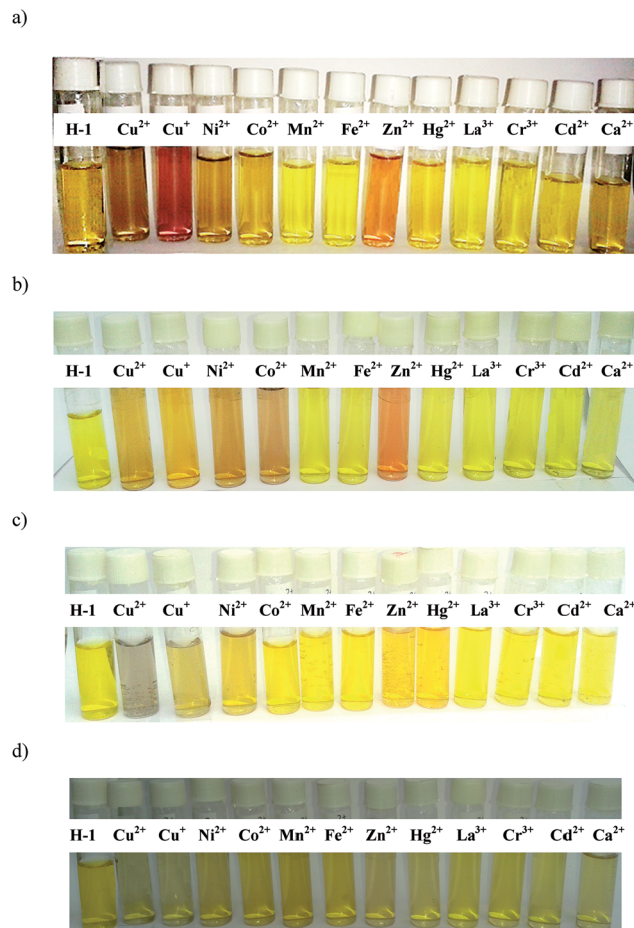
a)

b)

c)

d)

Fig. 11 (a) Color changes observed to chemosensor H-1 (2.5×10^{-4} M) with metal ions (2.5×10^{-4} M) in methanol. (b) Color changes observed to chemosensor H-1 (2.5×10^{-4} M) with metal ions (2.5×10^{-4} M) in methanol–triethylamine. (c) Color changes observed to chemosensor H-1 (2.5×10^{-4} M) with metal ions (2.5×10^{-4} M) in methanol–water media. (d) Color changes observed to chemosensor H-1 (2.5×10^{-4} M) with metal ions (2.5×10^{-4} M) in methanol–triethylamine–water.

a)

b)

c)

d)

Fig. 12 (a) Color changes observed to chemosensor H-3 (2.5×10^{-4} M) with metal ions (2.5×10^{-4} M) in methanol. (b) Color changes observed to chemosensor H-3 (2.5×10^{-4} M) with metal ions (2.5×10^{-4} M) in methanol–triethylamine. (c) Color changes observed to chemosensor H-3 (2.5×10^{-4} M) with metal ions (2.5×10^{-4} M) in methanol–water. (d) Color changes observed to chemosensor H-3 (2.5×10^{-4} M) with metal ions (2.5×10^{-4} M) in methanol–triethylamine–water.

Cu^{2+} in methanol, methanol–triethylamine and methanol–water solvent mixture the stoichiometry was shown to be in 1 : 1 proportions. H-1 and H-3 ligands coordinating in tridentate manner with two nitrogen and a quinonoid oxygen bound to metal ions. The tetrahedral 1 : 1 complex Cu^{2+} and 1 : 2 octahedral complex of Ni^{2+} was proposed for such type of ligands.[40,41]

Association constant of Cu^{2+} ion was determined using the Stern–Volmer plots from fluorescence experiments (Fig. S13 (for H-1) and Fig. S17 (for H-3) in ESI†). The concentrations of H-1 or H-3 used were 5×10^{-4} M and that for the metal being 1×10^{-3} M. The methanol solutions were used. The association constants (K_a) for H-1 turned out to be 4932 M^{-1} for Cu^{2+} whereas that for the Ni^{2+} was 1542 M^{-1} (Fig. S13a and b in ESI†). Likewise the association constants (K_a) for H-3 were observed to be 938.9 M^{-1} and 790.7 M^{-1} respectively, for Cu^{2+} and Ni^{2+}.

A competitive binding of metal ions was further studied through experiments in which equal volumes of H-1 and H-3
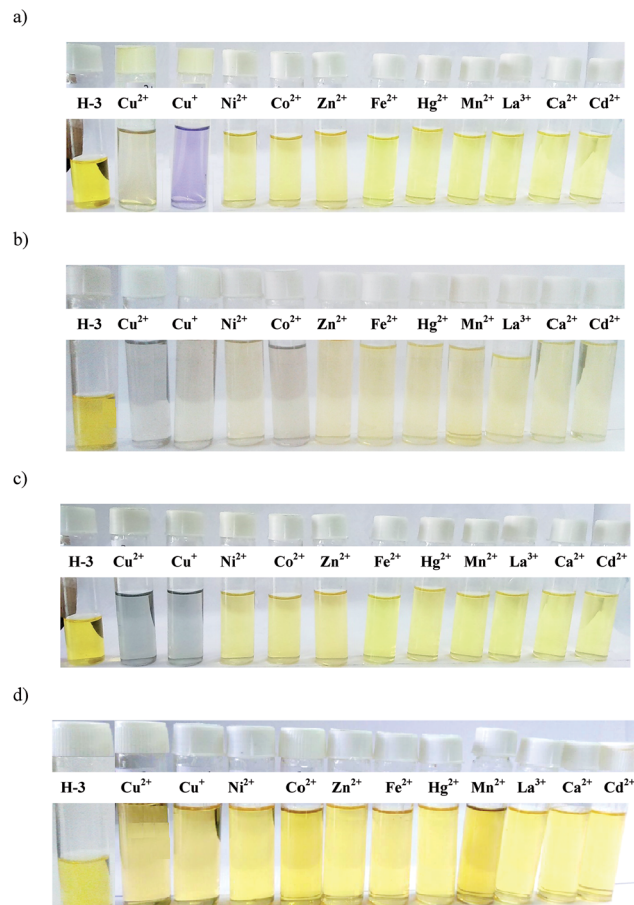
(1×10^{-4} M) were mixed with those of Cu^{2+}, Ni^{2+} and Co^{2+} (1×10^{-3} M). Noticeable colour changes can be noticed in solution mixture of metal ions (Fig. 14 and S18 in ESI†) for H-1 and H-3. UV-visible (Fig. S19 in ESI†) and fluorescence spectra of selected metal ion are displayed in Fig. 15. Ligands H-1 and H-3 are fluorescent and showed low quantum yields of 0.99% and 1.89%, respectively. Noteworthy enough, Cu^{2+} demonstrate significant fluorescence quenching for H-1 and H-3. The experiments further showed Ni^{2+} and Co^{2+} bring about competitive binding to H-1 and H-3 however Cu^{2+} prevailing over other metal ions which is in accordance with its large binding constant.

pH dependent metal ion binding experiments of H-1 and H-3 were carried out on metal ions Zn^{2+}, Cu^{2+}, Ni^{2+} and Co^{2+} in buffer solution of pH 4, 7 and 9. The metal ion binding was observed only in the basic pH (Fig. S20 in ESI†) and not for pH = 4.

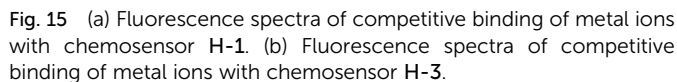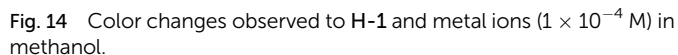The limit of detection (LOD) from the fluorescence experiments[42,43] with Cu^{2+} and H-1 or H-3 ligands are observed to be 1.48×10^{-8} mol L^{-1} for H-1 (Fig. S21 in ESI†) and 1.59×10^{-8} mol L^{-1} (Fig. S22 in ESI†) for H-3.

Fig. 13 (a) UV-visible spectra of **H-1** in presence of various metal ions in methanol. (b) UV-visible spectra of **H-1** in presence of various metal ions in methanol–triethylamine. (c) UV-visible spectra of **H-1** in presence of various metal ions in methanol : water media. (d) UV-visual spectra of **H-1** in presence of various metal ions in methanol–TEA–water.

DFT investigations

Optimized structures of aminonaphthoquinone derivatives obtained from the M06-2X based density functional theory are depicted in Fig. 16. Selected bond distances and angles are compared with X-ray crystal data in Table 3. As shown the overall structural parameters agree well with the experiments. A comparison of **H-1** and **H-2** shows that carbonyl C(1)O(1) bond distances are marginally elongated on substitution of thiophene instead of pyridine.

Structural ramifications in vibration frequencies are analyzed. Calculated vibrational frequencies of **H-1**, **H-2**, **H-3** and **H-4** are compared with the experiment in Table 4. As may be inferred the N–H stretching assigned to 3247 cm^{-1} of **H-1** engenders the frequency up shift of ~42 cm^{-1} for the ethyl substituted **H-3**. As oppose to this in case of thiophene on substitution of the ethyl functionality engender the lowering of

Fig. 14 Color changes observed to **H-1** and metal ions (1×10^{-4} M) in methanol.

Fig. 15 (a) Fluorescence spectra of competitive binding of metal ions with chemosensor **H-1**. (b) Fluorescence spectra of competitive binding of metal ions with chemosensor **H-3**.
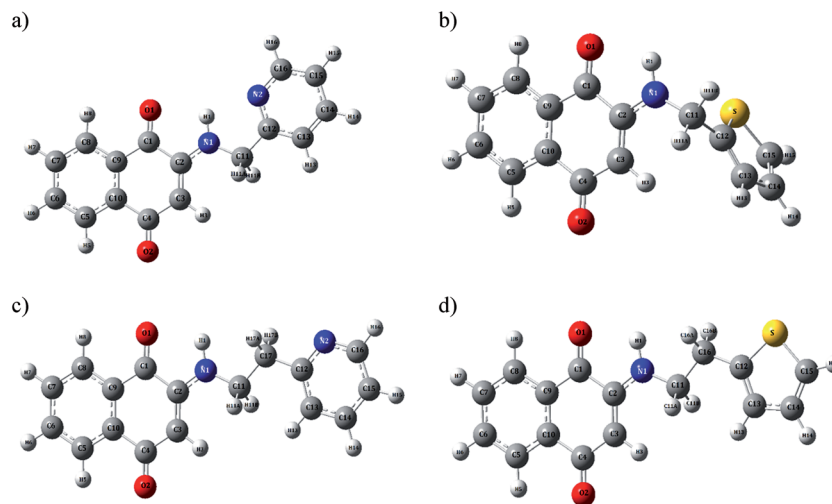
Fig. 16 Optimized geometries of (a) **H-1**, (b) **H-2**, (c) **H-3** and (d) **H-4**.

Table 3 Selected bond distances (in Å) in **H-1**, **H-2**, **H-3** and **H-4**

	H-1		H-3		H-4	
	Theo.	Obs.	Theo.	Obs.	Theo.	Obs.
C=O$_1$	1.209	1.219	1.210	1.220	1.211	1.219
C=O$_2$	1.217	1.234	1.216	1.237	1.216	1.246
C3–H3	1.083	0.950	1.083	0.950	1.083	0.950
N1–H1	1.015	0.880	1.012	0.880	1.012	0.880

Table 4 Selected vibrational frequencies in cm^{-1} (ν) of **H-1** to **H-4** scaled by factor 0.91

	H-1		H-2		H-3		H-4	
	Theo.	Obs.	Theo.	Obs.	Theo.	Obs.	Theo.	Obs.
ν(N1–H1)	3247	3355	3311	3354	3289	3336	3285	3338
ν(C3–H3)	2936	3061	2926	3061	2921	2960	2911	2915
ν(C=O$_1$)	1650	1672	1645	1670	1649	1672	1645	1669
ν(C=O$_2$)	1610	1632	1620	—	1617	1600	1618	—
ν(C=C)	1541	1593	1541	1599	1539	1570	1538	1593

Table 5 ^{1}H chemical shift (in ppm) in solvent and observed ^{1}H chemical shifts

	H-1		H-2		H-3		H-4	
	Theo.	Obs.	Theo.	Obs.	Theo.	Obs.	Theo.	Obs.
H1	8.1	8.08	6.5	8.11	5.6	7.62	5.6	7.55
H3	6.2	5.59	6.1	5.74	6.2	5.71	6.2	5.72
H5	8.4	7.90	9.0	7.90	8.4	7.92	8.4	7.33
H6	9.0	7.81	8.6	7.80	9.0	7.81	8.9	7.72
H7	8.6	7.77	8.5	7.71	9.0	7.70	9.1	7.82
H8	9.4	8.00	9.1	7.97	9.3	7.95	9.3	7.93
H11	4.6	4.52	4.9	4.61	3.6	3.54	3.6	3.45
H13	8.3	7.37	7.7	7.10	7.7	7.32	7.3	6.94
H14	8.5	7.73	7.7	6.97	8.5	7.72	7.6	6.96
H15	8.0	7.30	8.1	7.40	8.1	7.23	8.2	7.97
H16	9.7	8.55			9.6	8.51	3.4	3.12
H17					3.6	3.04		

frequency from 3311 cm^{-1} (**H-2**) to 3285 cm^{-1} (**H-4**). The inferences borne out from DFT are thus in consonance with the experiment.

^{1}H-NMR chemical shifts (δ_H) in **H-1**, **H-2**, **H-3** and **H-4** in DMSO (as solvent) were simulated through the SCRF-PCM theory. A comparison with the experiment is given in Table 5. The H(1) proton participating in N–H···O and N–H···N interactions in **H-1** emerge with relatively large deshielding (8.1 ppm) in the spectra. The signals of the corresponding proton in the rest of aminonaphthoquinone derivatives facilitate the N–H···O interactions and appear at ∼6.5 ppm. The alkyl protons emerge with up-field δ_H signals in the calculated ^{1}H NMR. These inferences on the calculated δ_H values concur with the experiment.
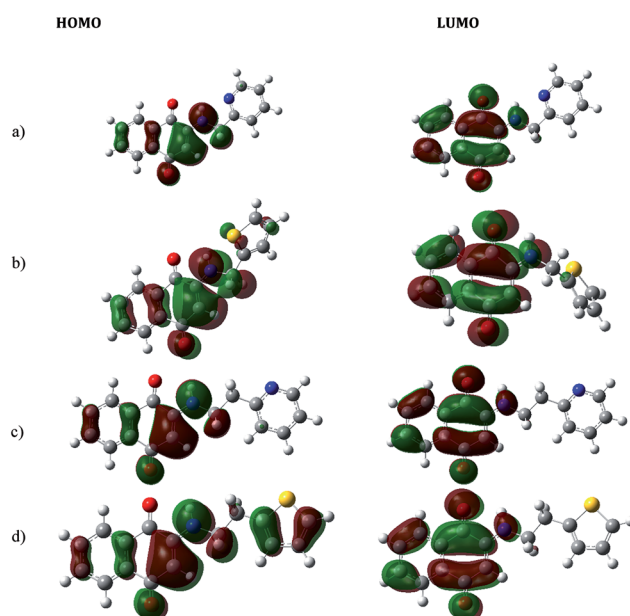

Fig. 17 Fronteir molecular orbitals of (a) **H-1**, (b) **H-2**, (c) **H-3** and (d) **H-4**.

Table 6 HOMO, LUMO gap (in eV) and global indices in H-1, H-2, H-3 and H-4

Molecular properties	H-1	H-2	H-3	H-4
$\Delta E_{HOMO-LUMO}$	5.6	5.6	5.7	5.6
Global hardness (η)	2.8	2.8	2.9	2.8
Electronic chemical potential (μ)	4.7	4.9	4.9	4.9
Electronegativity (χ)	4.7	4.9	4.9	4.9
Global electrophilicity index (ω)	4.0	4.3	4.3	4.3

The molecular Frontier orbital's HOMO and LUMO (isosurface of ± 0.04 au) in aminonaphthoquinone ligands are portrayed in Fig. 17. The complimentarily of charge distributions between HOMO and LUMO is thus transparent. The electronic absorption spectra except **H-4** revealed the band near ~336 nm assigned to the HOMO to LUMO transition. The HOMO–LUMO energies, global indices of reactivity, namely, chemical potential (μ), hardness (η), and electrophillicity index (ω), are summarized in Table 6.

Conclusions

Naphthoquinone based chemosensors are characterized from the X-ray diffraction and spectroscopy experiments in conjunction with the density functional theory. X-ray diffraction experiments revealed the C–H⋯π interactions in molecular packing those bring about a variation in their optical properties. The metal ion binding of **H-1** and **H-3** in methanol, methanol–water mixture and in the presence of mild base triethylamine were examined. The binding of **H-1** and **H-3** with Cu^{2+} revealed 1 : 1 stoichiometry in methanol water mixture compared to that of Ni^{2+} which was 1 : 2 proportions when the methanol or methanol–triethylamine mixture were used. The association constant of Cu^{2+} with **H-1** was observed to be ~5.2 times as larger than that for the **H-3**. Secondly, the ligands **H-1** and **H-3** display remarkable recognition ability toward the Cu^{2+}, Ni^{2+}, Co^{2+} ions in methanol. Both ligands showed remarkable selectivity in the detection of Cu^{2+} in methanol/H_2O solution. The experimental investigations further were corroborated through the inferences drawn based on the ^1H NMR and infrared spectra derived from the density functional theory.

Conflicts of interest

There are no conflicts to declare.

Acknowledgements

References

1 L. Li, E. Leyva and R. Las Garcia, *Rev. Mex. Cienc. Farm.*, 2011, **42**, 6–17.

2 R. P. Varma, *Med. Chem.*, 2006, **6**, 489–499.

3 H. R. Lawrence, A. Kazi, Y. Luo, R. Kendig, Y. Ge, S. Jain, K. Daniel, D. Santiago, W. C. Guida and S. M. Sebti, *Bioorg. Med. Chem.*, 2007, **18**, 5576–5592.

4 V. K. Tandon, H. K. Maurya, A. Tripathi, G. B. Shivakeshava, P. V. Shukla, P. Srivastava and D. Panda, *Eur. J. Med. Chem.*, 2009, **44**, 1088–1092.

5 E. H. da Cruz, C. M. Hussene, G. G. Dias, E. B. Diogo, I. M. de Melo, B. L. Rodrigues, M. G. da Goukrt, B. C. Cavalcanti, C. Pessoa and E. N. da Silva Junior, *Bioorg. Med. Chem.*, 2014, **22**, 1609–1619.

6 H. R. Nasiri, M. G. Madej, R. Panisch, M. Lafontaine, J. W. Bats, C. R. Lancaster and H. Schwalbe, *J. Med. Chem.*, 2013, **56**, 9530–9541.

7 D. Bhasin, S. N. Chettiar, J. P. Etter, M. Mok and P. K. Li, *Bioorg. Med. Chem.*, 2013, **21**, 4662–4669.

8 C. V. Ryu and D. H. Kim, *Arch. Pharmacal Res.*, 1992, **15**, 263–268.

9 V. K. Tandon, H. K. Maurya, N. N. Mishra and P. K. Shukla, *Eur. J. Med. Chem.*, 2009, **44**, 3130–3137.

10 J. J. Inbaraj and C. F. Chignell, *Chem. Res. Toxicol.*, 2004, **17**, 55–62.

11 V. K. Tandon, R. B. Chhor, R. V. Singh, S. Raj and D. B. Yadav, *Bioorg. Med. Chem. Lett.*, 2004, **14**, 1079–1083.

12 K. Sasaki, H. Abe and F. Yoshizaki, *Biol. Pharm. Bull.l*, 2002, **25**, 669–670.

13 V. K. Tandon, D. B. Yadav, H. K. Maurya, A. K. Chaturvedi and P. K. Shukla, *Bioorg. Med. Chem.*, 2006, **14**, 6120–6126.

14 T. Kayashima, M. Mori, H. Yoshida, Y. Mizushina and K. Matsubara, *Cancer Lett.*, 2009, **278**, 34–40.

15 E. N. Da Silva Jr, D. F. de Deus, B. C. Cavalcanti, C. Pessoa, L. V. Costa-Lotufo, R. C. Motenegro, M. O. de Moraes, M. C. E. R. Pinto, C. A. de Simone, V. F. Fereira, M. O. F. Goulart, C. K. Z. Andrade and A. V. Pinto, *J. Med. Chem.*, 2010, **53**, 504–508.

16 O. D. Zakharova, L. P. Ovchinnikova, L. I. Goryunov, N. M. Troshkova, V. D. Shteingarts and G. A. Nevinsky, *Eur. J. Med. Chem.*, 2010, **45**, 2321–2326.

17 J. Benites, J. A. Valderrama, K. Bettega, R. C. Pedrosa, P. B. Calderon and J. Verrax, *Eur. J. Med. Chem.*, 2010, **45**, 6052–6057.

18 N. Pradidphol, N. Kongakathip, P. Sittikul, N. Boonyalai and B. Kongkathip, *Eur. J. Med. Chem.*, 2012, **49**, 253–270.

19 V. K. Tandon, R. V. Singh, S. Raj, R. B. Chhor and Z. K. Khan, *Boll. Chim. Farm.*, 2002, **141**, 304–310.

20 T. V. Ilina, E. A. Semenova, T. R. Pronyaeva, A. G. Pokrovskii, I. N. Nechepurenko, E. E. Shults, O. I. Anderrva, S. N. Kochetkov and G. A. Tolstikov, *Dokl. Biochem. Biophys.*, 2002, **382**, 56–59.

21 A. J. M. da Silva, C. D. Buarque, F. V. Brito, L. Aurelian, L. F. Macedo, L. H. Malkas, R. J. Hickey, D. V. S. Lopes, Y. L. B. Murakami, N. M. V. Silva, P. A. Melo,

R. R. B. Laruso, N. G. Castro and P. R. R. Costa, *Bioorg. Med. Chem.*, 2002, **10**, 2731–2738.

22 E. N. da Silva, M. Cecillia, B. V. de Souza, A. V. Pinto, F. R. Pinto, M. O. F. Goulart, F. W. A. Barros, C. Pessoa, L. V. Costa-Lotufa, R. C. Montenegro, M. Moraesel and V. F. Ferreiraa, *Bioorg. Med. Chem.*, 2007, **15**, 7035–7042.

23 M. A. Maetinez, G. Uevas, M. J. Estrada, I. Gonzalez, B. L. Hennasen and N. M. Ruvalcaba, *J. Org. Chem.*, 1999, **64**, 3684–3694.

24 (*a*) Z. Xu, Y. Xiao, X. Qian, J. Cui and D. Cui, *Org. Lett.*, 2005, **7**, 889–892; (*b*) Y. Kubo, M. Ymamoto, M. Ikeda, M. Takeuchi, S. Shinkai, S. Yamaguchi and K. Tamao, *Angew. Chem., Int. Ed.*, 2003, **42**, 2036–2040.

25 D. D. Perrin, W. L. Armarego and D. R. Perrin, *Purification of Laboratory Chemicals*, Pergamon Press, London, 1988, p. 260.

26 *Bruker, APEX2, SAINT and SADABS*, Bruker AXS Inc, Madison, Wisconsin, USA, 2007.

27 G. M. Sheldrick, *Acta Crystallogr., Sect. A: Found. Crystallogr.*, 2008, **64**, 112–122.

28 L. J. Farrugia, *J. Appl. Crystallogr.*, 2012, **45**, 849–854.

29 C. F. Macrae, I. J. Bruno, J. A. Chisholm, P. R. Edgington, P. McCabe, E. Pidcock, L. Rodriguez-Monge, R. Taylor, J. Van de Streek and P. A. Wood, *J. Appl. Crystallogr.*, 2008, **41**, 466–470.

30 L. R. Monge, R. Taylor, J. van de Streek and P. A. Wood, *J. Appl. Crystallogr.*, 2008, **41**, 466–470.

31 L. Spek, *Acta Crystallogr., Sect. D: Biol. Crystallogr.*, 2009, **65**, 148–155.

32 M. J. Frisch, G. W. Trucks, H. B. Schlegel, G. E. Scuseria, M. A. Robb, J. R. Cheeseman, J. A. Montgomery Jr, T. Vreven, K. N. Kudin, J. C. Burant, J. M. Millam, S. S. Iyengar, J. Tomasi, V. Barone, B. Mennucci, M. Cossi, G. Scalmani, N. Rega, G. A. Petersson, H. Nakatsuji, M. Hada, M. Ehara, K. Toyota, R. Fukuda, J. Hasegawa, M. Ishida, T. Akajima, Y. Honda, O. Kitao, H. Nakai, M. Klene, X. Li, J. E. Knox, H. P. Hratchian, J. B. Cross, V. Bakken, C. Adamo, J. Jaramillo, R. Gomperts, R. E. Stratmann, O. Yazyev, A. J. Austin, R. Cammi, C. Pomelli, J. W. Ochterski, P. Y. Ayala, K. Morokuma, G. A. Voth, P. Salvador, J. J. Dannenberg, V. G. Zakrzewski, S. Dapprich, A. D. Daniels, M. C. Strain, O. Farkas, D. K. Malick, A. D. Rabuck, K. Raghavachari, J. B. Foresman, J. V. Ortiz, Q. Cui, A. G. Baboul, S. Clifford, J. Cioslowski, B. B. Stefanov, G. Liu, A. Liashenko, P. Piskorz, I. Komaromi, R. L. Martin, D. J. Fox, T. Keith, M. A. Al-Laham, C. Y. Peng, A. Nanayakkara, M. Challacombe, P. M. W. Gill, B. Johnson, W. Chen, M. W. Wong, C. Gonzalez and J. A. Pople, *Gaussian03, revision*, Gaussian, Inc., Pittsburgh, PA, 2003.

33 R. Patil, D. Chadar, D. Chaudhari, J. Peter, M. Nikalje, T. Weyhermüller and S. Salunke-Gawali, *J. Mol. Struct.*, 2014, **1075**, 345–351.

34 S. Salunke-Gawali, L. Kathawate, Y. Shinde, V. G. Puranik and T. Weyhermüller, *J. Mol. Struct.*, 2012, **1010**, 38–45.

35 S. Salunke-Gawali, O. Pawar, M. Nikalje, R. Patil, T. Weyhermüller, V. G. Puranik and V. B. Konkimalla, *J. Mol. Struct.*, 2014, **1056–1057**, 97–103.

36 S. Salunke-Gawali, L. Kathawate and V. G. Puranik, *J. Mol. Struct.*, 2012, **1022**, 189–196.

37 S. Salunke-Gawali, S. Y. Rane, V. G. Puranik, C. Guyard-Duhayan and F. Varret, *Polyhedron*, 2004, **23**, 2541–2547.

38 S. Pal, M. Jadhav, T. Weyhermüller, Y. Patil, M. Nethaji, U. Kasabe, L. Kathawate, V. Badireenath Konkimalla and S. Salunke-Gawali, *J. Mol. Struct.*, 2013, **1049**, 355–361.

39 A. P. Ware, A. Patil, S. Khomane, T. Weyhermüller, S. S. Pingale and S. Salunke-Gawali, *J. Mol. Struct.*, 2015, **1093**, 39–48.

40 A. Patil, D. Lande, A. Nalkar, S. P. Gejji, D. Chakravarty, R. Gonnade, T. Moniz, M. Rangel, E. Periera and S. Salunke-Gawali, *J. Mol. Struct.*, 2017, **1143**, 495–514.

41 G. Agarwal, D. N. Lande, D. Chakravarty, S. P. Gejji, P. Gosavi-Mirkute, A. Patil and S. Salunke-Gawali, *RSC Adv.*, 2016, **6**, 88010–88029.

42 Q. Lin, T. Lu, X. Zhu, T. Wei, H. Li and Y. Zhang, *Chem. Sci.*, 2016, **7**, 5341–5346.

43 Q. Lin, P. Mao, Y. Fan, L. Liu, J. Liu, Y. Zhang, H. Yao and T. Wei, *Soft Matter*, 2017, **13**, 7085–7089.